Received 4 October 2025; accepted 16 October 2025. Date of publication 22 October 2025; date of current version 11 November 2025. The review of this article was coordinated by Editor Chenhao Qi.

Digital Object Identifier 10.1109/OJVT.2025.3623883

# **Iterative Soft-MMSE Detection Aided AFDM and OTFS**

HUGO HAWKINS (Graduate Student Member, IEEE), CHAO XU (Senior Member, IEEE), LIE-LIANG YANG (Fellow, IEEE), AND LAJOS HANZO (Life Fellow, IEEE)

School of Electronics and Computer Science, University of Southampton, SO171BJ Southampton, U.K.

CORRESPONDING AUTHOR: LAJOS HANZO (e-mail: lh@ecs.soton.ac.uk).

This work was supported in part by the Platform for Driving Ultimate Connectivity (TITAN) under Grant EP/X04047X/1 and Grant EP/Y037243/1, in part by Robust and Reliable Quantum Computing (RoaRQ) under Grant EP/W032635/1 and Grant PerCom EP/X012301/1, and in part by India–UK Intelligent Spectrum Innovation ICON under Grant UKRI-1859 for Engineering and Physical Sciences Research Council (EPSRC) Projects

**ABSTRACT** Affine Frequency Division Multiplexing (AFDM) has attracted substantial research interest due to its implementational similarity to Orthogonal Frequency-Division Multiplexing (OFDM), whilst attaining comparable performance to Orthogonal Time Frequency Space (OTFS). Hence, we embark on an in-depth performance characterisation of coded AFDM and of its equivalent OTFS counterpart. Soft-Minimum Mean Square Error (MMSE) reception taking into account a priori probabilities in the weighting matrix is applied in conjunction with Recursive Systematic Convolutional (RSC)- and RSCUnity Rate Convolutional (URC) coding to AFDM. Iterative decoding convergence analysis is carried out with the aid of the powerful semianalytical tool of EXtrinsic Information Transfer (EXIT) chart, and its Bit Error Rate (BER) performance is compared to OFDM and to the equivalent OTFS configurations. As there are no consistent configurations of AFDM and OTFS utilised in the literature to compare their relative performances, two AFDM configurations and three OTFS configurations are considered. The results show that the BER of AFDM is lower than that of the equivalent OTFS configurations at high Energy per bit over Noise power  $(E_b/N_0)$  for small system matrix dimensions, for a low number of iterations, and for high code rates. In all other cases, the BER of AFDM is shown to be similar to that of its equivalent OTFS configurations. Given that the RSC BER performance fails to improve beyond two iterations, this solution is recommended for low-complexity transceivers. By contrast, if the extra complexity of the RSC-URC aided transceiver is affordable, an extra (E<sub>b</sub>/N<sub>0</sub>) gain of 1.8 dB may be attained at a BER of  $10^{-5}$  and a code rate of 0.5.

**INDEX TERMS** Affine frequency division multiplexing, orthogonal frequency-division multiplexing, orthogonal time frequency space, recursive systematic convolutional codes, soft-minimum mean square error, unity rate convolutional codes.

# I. STATE-OF-THE-ART, MOTIVATION, AND CONTRIBUTIONS

Affine Frequency Division Multiplexing (AFDM) is a novel chirp-based waveform [1], and it may be deemed reminiscent of Orthogonal Frequency-Division Multiplexing (OFDM), where the Discrete Fourier Transform (DFT) is replaced by the Discrete Affine Fourier Transform (DAFT). The DAFT is a generalised transform, with the DFT being a specific form of the DAFT. It is characterised by two chirp parameters, namely chirp parameter 1  $(c_1)$  and chirp parameter 2  $(c_2)$ , which can be flexibly tuned for optimising the diversity and correlation

properties of the signal. Other forms of OFDM utilising the DAFT [2] or chirps [3], [4] have been proposed, but these still lead to propagation paths being separable only by delay, not Doppler shift. By contrast, the DAFT utilised in Affine Frequency Division Multiplexing (AFDM) is specifically configured to ensure that the propagation paths are separable by both delay and Doppler shift, similar to Orthogonal Time Frequency Space (OTFS) schemes [5], [6]. This allows AFDM to achieve full diversity, like OTFS. The communication performance of AFDM has also been shown to be similar to that of OTFS [1]. However, the maximum Doppler shift must

be known at the transmitter to configure the DAFT. AFDM also requires a prefix to be added, the Chirp Periodic Prefix (CPP), similarly to the OFDM Cyclic Prefix (CP). The CPP reduces to a CP if the value of  $c_1$  for the DAFT meets certain conditions. The correct configuration of the DAFT allows the Affine Frequency Domain (AFD) channel matrix to be sparse, similar to the OTFS Delay-Doppler Domain (DD) channel matrix, but with a different structure.

The similarities between OFDM and AFDM have led to research in many areas of communication [7], such as satellite communication [8], secure transmission [9], [10], and DFT-based AFDM [11]. The DFT-based AFDM may be viewed as a precoded OFDM scheme, to align its implementation more closely to that of OFDM [11].

#### A. SPECTRAL EFFICIENCY

AFDM has been shown to possess a higher spectral efficiency than OTFS when conventional pilot symbol-based channel estimation is employed [12], [13], [14]. This is due to the lower number of guard symbols required by AFDM compared to OTFS, as AFDM is a single-domain waveform, whereas OTFS requires guard symbols along both the delay and Doppler domains. However, this spectral efficiency improvement is not seen when other pilot methods are harnessed [15], [16]. For example, when superimposed pilot symbols are considered, this spectral efficiency improvement is no longer observed [15], but superimposed symbols require more complex detection methods for mitigating the interference between pilot and data symbols.

## B. PEAK TO AVERAGE POWER RATIO

As a drawback, AFDM suffers from high Peak to Average Power Ratio (PAPR), as its structure is similar to OFDM, but it can be reduced by adjusting  $c_2$  of the DAFT [17]. This creates a DAFT with multiple groups of  $c_2$  values within the transform. The authors show that increasing the number of chirp parameter groups decreases the PAPR. This variability in the transmit DAFT leads to a higher Bit Error Rate (BER), when the receiver does not know which  $c_2$  values have been employed. Reddy et al. [18] propose to reduce the PAPR by applying  $\mu$ -law companding and decompanding in the Time Domain (TD), prior to transmission and after reception respectively. This  $\mu$ -law companding reduces the PAPR of AFDM to a greater extent than the method in [17], with no substantial impact on the BER for moderate companding.

# C. INDEX MODULATION

As for OTFS and OFDM, there has also been keen interest in the combination of AFDM and Index Modulation (IM) [19], [20], [21], [22], [23]. Standard IM applied to AFDM has been shown to slightly reduce the BER of AFDM [19] for both coded and uncoded transmission. This combination has been extended to a multi-antenna scenario in [20], where the transmission from each antenna is shifted by a fixed delay. The addition of IM is shown to reduce the BER of AFDM

in this scenario, albeit at the expense of additional complexity. As expected, the BER of the cyclic transmission method decreases as the number of transmit antennas is increased.

Applying IM to the DAFT parameters has also been proposed [21]. The values of  $c_2$  within groups are varied based on the input bits, in a similar manner to standard IM. This method is shown to result in a lower BER than standard AFDM-IM for Maximum Likelihood (ML) detection. Another innovative IM scheme relies on Walsh-Hadamard sequence based spreading [22]. This is applied on a per-group basis of chirp subcarriers, and it is shown to lead to a lower BER than both AFDM and standard AFDM-IM for a given throughput at sufficiently high Signal to Noise Ratios (SNRs).

#### D. SPARSE CODE MULTIPLE ACCESS

The employment of spreading sequences has also been investigated in multi-user communication. Multi-user Sparse Code Multiple Access (SCMA) aided AFDM is proposed in [24], for both uplink and downlink communications. The authors develop a SCMA codebook design to simplify the input-output relationship in the AFD, thereby allowing for a simpler receiver. The detector proposed for coded transmission iterates between a linear Minimum Mean Square Error (MMSE) receiver and a Low-Density Parity-Check (LDPC) decoder, whose performance is enhanced by the addition of orthogonal approximate message passing. The uncoded and coded AFDM-SCMA schemes are shown to consistently outperform the equivalent OFDM schemes in both uplink and downlink transmission. The equivalent OTFS schemes are shown to have a similar performance to their AFDM counterparts.

#### E. INTEGRATED SENSING AND COMMUNICATION

As Integrated Sensing and Communication (ISAC) is a subject that attracts considerable interest, research into the employment of AFDM in this field is also ongoing [25], [26], [27], [28], [29], [30], [31], [32], [33]. An overview and comparison of various waveforms, including OTFS and AFDM, is presented in [25], for various key ISAC performance indicators. The authors show that AFDM inherits a variety of OFDM and OTFS characteristics in communication scenarios. Furthermore, diverse sensing characteristics may be attained due to the flexibility offered by tuning the values of the DAFT chirp parameters.

Ni et al. [26] consider monostatic AFDM ISAC. Multiple AFDM frames are transmitted and received, to produce a received signal matrix, in a similar manner to symbol cancellation-based OFDM ISAC [34]. A pair of detection algorithms are implemented. The first uses the TD signals, and utilises a method similar to symbol cancellation-based OFDM sensing. The second method processes the received Affine Frequency Domain (AFD) signal. The AFD method is shown to experience only small image SNR fluctuations as the Doppler shift is increased. By contrast, the image SNR of the TD and symbol cancellation-based OFDM methods degrades significantly as the Doppler shift is increased. The AFD method has a higher maximum unambiguous Doppler

shift than the TD method, and it is therefore capable of correctly estimating much higher velocities than the TD method. No comparison to OTFS sensing is presented.

Pilot symbol-based monostatic AFDM ISAC is considered in [27], where the pilot symbol is inserted into the transmit signal, with guard bands surrounding it to prevent interference between the pilot and data symbols, as in [12], [13]. Sensing is performed using the guard band and pilot symbol only. This allows for the low-complexity removal of the self-interference imposed by the transmitter on the receiver. This pilot-based sensing method is shown to reach the sensing error floor at a higher SNR than a full signal sensing method, but at a much lower complexity. The performance of AFDM pilot sensing is shown to be comparable to that of OTFS sensing, but the latter employs a more complex interference cancellation method.

Both a monostatic method and a bistatic method are presented in [29], for AFDM, OFDM, and OTFS, utilising probabilistic data association-based message passing and parametric bilinear Gaussian belief propagation, respectively. The performance of AFDM is shown to be similar to that of OTFS, but exhibiting a slightly lower BER and channel parameter MMSE at higher SNRs.

Xiao et al. [30] develop an AFDM sensing method relying on prior knowledge of the channel's delay profile, when assuming that the number of resolvable paths as well as the relative delays between resolvable paths are known, and that there is a single target. This information is leveraged to estimate the target parameters under the assumption that their statistical distributions follow a Nakagami-m distribution. The proposed method is shown to leverage Non-Line of Sight (NLoS) path information, leading to a reduced estimation error, and to an increased robustness to incorrect information. Nonetheless, the performance of the proposed method is more vulnerable to degradation caused by increases in target velocity than the benchmark algorithm.

A super-imposed pilot based method is proposed in [31] for AFDM monostatic ISAC and bistatic channel estimation. Channel estimation is performed by an MMSE algorithm, whilst target parameter estimation is achieved by implementing a TD compensation-based correlation method. The pilot symbols used are Zadoff-Chu sequences. The results presented show that the proposed system is capable of outperforming other pilot-based channel estimation methods, including the method of [15]. In contrast to [15], the proposed pilot arrangement performance does not significantly deteriorate when large delays are present. The pilot arrangement of [31] also leads to a lower incorrect detection probability than that of [15]. No comparison is offered to illustrate the target parameter estimation error performance.

## F. ITERATIVE EQUALISATION AND CHANNEL CODING

Due to the relative novelty of AFDM, there is a paucity of publications investigating the benefits of iterative equalisation and channel coding on the performance of AFDM. Nonetheless, a low complexity iterative linear-MMSE-based equalisation method is proposed for AFDM in [35]. The authors first

determine the optimum DAFT chirp parameter values to minimise the BER when MMSE equalisation is employed. An iterative TD MMSE method is developed to reduce the complexity of soft linear-MMSE detection. The authors show that the proposed chirp parameter selection method allows the system to reach the BER lower bound. This advantage becomes more apparent when the propagation channel is doubly selective. The proposed iterative TD MMSE method is shown to have a slightly higher BER than iterative linear-MMSE. The performances of AFDM and OTFS are similar to each other for both equalisation methods. Soft-MMSE has also been utilised to improve the BER performance of AFDM in wideband channels [36].

Channel coding has also been investigated in [19], [37]. Xu et al. [37] develop a multi-block unitary transform-based approximate message passing algorithm for AFDM under fractional delay and Doppler indices. Fractional delay indices are scarcely covered in the AFDM literature. This algorithm is conceived to mitigate the energy dispersion effects of the fractional channel indices on the received signal. The proposed algorithm is shown to exhibit a higher iterative gain, illustrated by "empirical" EXtrinsic Information Transfer (EXIT) chart analysis, and a lower BER than the Gaussian approximate message passing benchmark. This algorithm also allows AFDM to exhibit a lower BER than OTFS, since AFDM only experiences interference in a single dimension, as opposed to two dimensions for OTFS. Channel coding was not the focus of the contributions of [19] and [37].

The only currently published work that considers the combination of iterative equalisation and channel coding for AFDM communication is [24]. The soft-MMSE method implemented is specifically designed for SCMA, and hence is not generally applicable to AFDM systems.

## G. MOTIVATION AND CONTRIBUTIONS

As discussed above, AFDM has attracted substantial interest due to its similarity in implementation to OFDM, whilst allowing for comparable performance to OTFS. Although some publications consider coded AFDM and soft-MMSE, there is no in-depth comparison of coded AFDM to its equivalent OTFS counterpart. Hence, the current work addresses this knowledge gap. Table 1 boldly contrasts the novelties of the proposed system to the existing literature. The specific contributions of this work are detailed below:

• Firstly, a parametric study of the communication performance of OFDM, AFDM and OTFS in doubly selective fading is performed for both coded and uncoded transmission. Multiple OTFS and AFDM configurations, defined in Table 2, are investigated, since the existing publications tend to compare AFDM to OTFS with different subcarrier spacings and/or bandwidths [10], [13], [20]. OTFS 1 is the original OTFS configuration of [5], [6] whose subcarrier spacing and number of subcarriers are identical to OFDM. The AFDM 1 scheme of [1], [12], [13] is equivalent to OTFS 1, where both schemes share the same matrix dimension. Furthermore,

**TABLE 1.** Comparison of Contributions From the Literature

| Papers<br>Topics   | [13] | [19]     | [20]     | [24]     | [29]     | [35] | [37]     | This work |
|--|------|----------|----------|----------|----------|------|----------|-----------|
| Topics   |      |          |          |          |          |      |          |           |
| System overview  |      |          |          |          |          |      |          |           |
| Doubly selective channel   | ✓    | ✓        | ✓        | <b>~</b> | <b>√</b> | ✓    | <b>√</b> | <b>✓</b>  |
| Channel coding   |      | ✓        |          | <b>✓</b> |          |      | <b>√</b> | <b>✓</b>  |
| Comparison between AFDM, OTFS and OFDM                             | ✓    |          |          | <b>✓</b> | <b>✓</b> | ✓    | <b>√</b> | <b>✓</b>  |
| Receive signal processing  |      |          |          |          |          |      |          |           |
| Iterative detection  |      |          | ✓        | <b>√</b> | <b>√</b> | ✓    | <b>√</b> | ✓         |
| Soft-MMSE  |      |          |          | <b>√</b> |          | ✓    |          | ✓         |
| URC code assisted decoding   |      |          |          |          |          |      |          | ✓         |
| Iterative soft-MMSE and RSC decoding                               |      |          |          |          |          |      |          | ✓         |
| Performance analysis   |      |          |          |          |          |      |          |           |
| EXIT chart and trajectory analysis                                 |      |          |          |          |          |      | <b>√</b> | ✓         |
| Scalable numerology for AFDM and OTFS configurations               |      | <b>√</b> | <b>√</b> |          |          |      |          | ✓         |
| Respective application domains of AFDM and OTFS configurations are |      |          |          |          |          |      |          | √         |
| identified   |      |          |          |          |          |      |          |           |

**TABLE 2. OFDM, OTFS and AFDM Configurations** 

|                  | OFDM                  | AFDM 1                               | OTFS 1                | AFDM 2                | OTFS 2                        | OTFS 3                              |
|------------------|-----------------------|--------------------------------------|-----------------------|-----------------------|-------------------------------|-------------------------------------|
| Dimension        | M                     | $\ddot{N}_1 = MN$                    | MN                    | M                     | $M_2N_2=M$                    | MN                                  |
| Subcarrier       | $\Delta f$            | $\Delta f_1 = \frac{\Delta f}{N}$    | $\Delta f$            | $\Delta f$            | $\Delta f_2 = N_2 \Delta f$   | $\Delta f_1$                        |
| spacing          |                       |                                      |                       |                       |                               |                                     |
| Bandwidth        | $M\Delta f$           | $\ddot{N}_1 \Delta f_1 = M \Delta f$ | $M\Delta f$           | $M\Delta f$           | $M_2 \Delta f_2 = M \Delta f$ | $M\Delta f_1 = \frac{M\Delta f}{N}$ |
| Duration         | T                     | $\frac{1}{\Delta f_1} = NT$          | NT                    | T                     | $\frac{N_2}{\Delta f_2} = T$  | $\frac{N}{\Delta f_1} = N^2 T$      |
| Delay resolution | $\frac{1}{M\Delta f}$ | $\frac{1}{M\Delta f}$                | $\frac{1}{M\Delta f}$ | $\frac{1}{M\Delta f}$ | $\frac{1}{M\Delta f}$         | $\frac{N}{M\Delta f}$               |
| Doppler          | $\frac{\Delta f}{N}$  | $\frac{\Delta f}{N}$                 | $\frac{\Delta f}{N}$  | $\Delta f$            | $\Delta f$                    | $\frac{\Delta f}{N^2}$              |
| resolution       |                       |                                      |                       |                       |                               |                                     |
| Throughput       | $B_S$                 | $B_S$                                | $B_S$                 | $B_S$                 | $B_S$                         | $\frac{B_S}{N}$                     |
| Complexity per   | M                     | MN                                   | MN                    | M                     | M                             | MN                                  |
| block            |                       |                                      |                       |                       |                               |                                     |
| References       | [8], [18], [19],      | [1], [10],                           | [1], [7],             | [7], [8], [11],       | [20]                          | [10], [24], [37]                    |
|                  | [21], [26]            | [12]–[15], [20],                     | [11]–[15], [28],      | [18], [19], [21],     |                               |                                     |
|                  |                       | [28], [32],                          | [32], [35], [36]      | [26]                  |                               |                                     |
|                  |                       | [35]–[37]                            |                       |                       |                               |                                     |

OTFS 2 [20] and AFDM 2 [15], [32], [35] have the same matrix dimension as a single OFDM symbol. These five configurations utilise the same bandwidth. The last configuration, OTFS 3 [10], [24], [37], has the same matrix dimension as OTFS 1, but its subcarrier spacing is identical to that of AFDM 1.

Secondly, a soft-MMSE equalisation method that is applicable to OFDM, AFDM and OTFS in an iterative turbo receiver architecture is proposed, that exchanges extrinsic information between the demapper and the channel decoder. Soft-MMSE refers to the holistic MMSE solution that updates its MMSE weighting matrix based on both the channel condition and the *a priori* probabilities gleaned from the channel decoder. EXIT chart analysis is performed to investigate the performance of Recursive Systematic Convolutional

- (RSC)-coded OFDM, AFDM and OTFS. Moreover, Unity Rate Convolutional (URC) coding is harnessed in order to improve the decoding convergence.
- It is demonstrated that for low-complexity transceivers having high coding rates, AFDM configurations exhibit a lower BER than their OTFS counterparts. Hence AFDM is better suited to low-complexity systems than OTFS at significant velocities.

#### H. NOTATIONS

In the following sections, italics are used for scalar values (a/A), vectors are in lower case bold (a), matrices are in upper case bold (A), the transpose operation is denoted by  $(\cdot)^T$ , the complex conjugate operation is denoted by  $(\cdot)^*$ , the complex conjugate/Hermitian transpose is  $(\cdot)^H$ , and the matrix inverse is  $(\cdot)^{-1}$ . DD variables are denoted with a tilde  $(\widetilde{a})$ , AFD

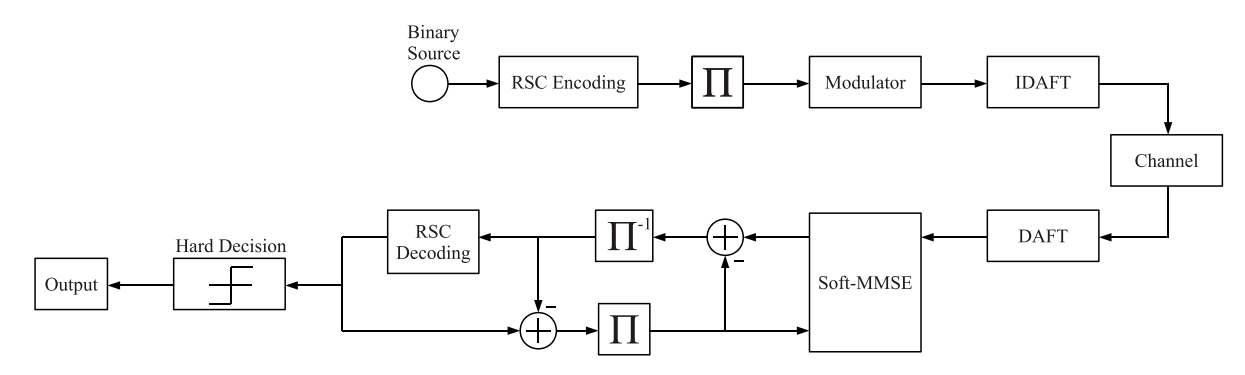


FIGURE 1. Block diagram of RSC-AFDM.

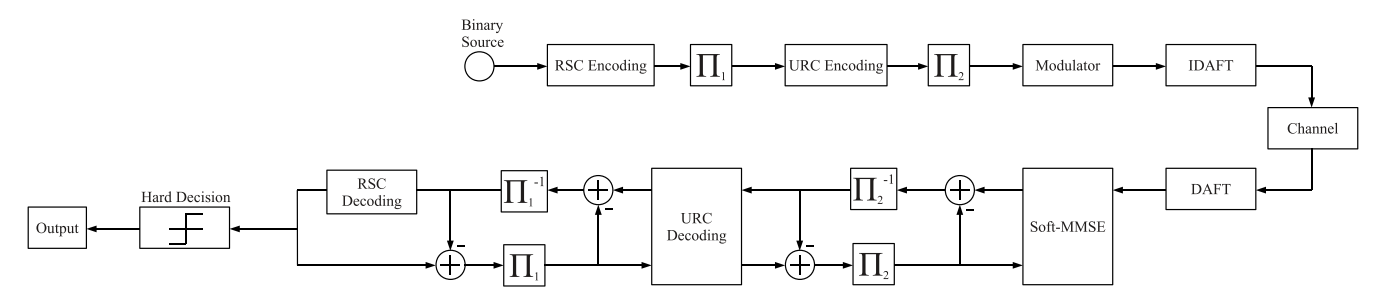


FIGURE 2. Block diagram of RSC-URC-AFDM.

variables with two dots  $(\ddot{a})$ , and TD variables are plain symbols (a).

# **II. TRANSMIT SIGNAL MODEL**

The data bit vector  $\boldsymbol{b}_D \in \mathbb{R}^{R_c B_S \ddot{N} \Xi \times 1}$  is encoded to produce the transmit bit vector  $\boldsymbol{b} \in \mathbb{R}^{B_S \ddot{N} \Xi \times 1}$ , where  $R_c$  is the channel coding rate,  $B_S = log_2(\Gamma)$  is the number of bits per symbol,  $\Gamma$  is the modulation order,  $\ddot{N}$  is the number of AFDM chirp subcarriers, and  $\Xi$  is the number of transmission blocks within a frame. A transmission block refers to a set of  $\ddot{N}$  symbols (or equivalent for other waveforms) sent by the transmitter, and the channel parameters are assumed to be constant for the  $\Xi$  transmission blocks within a frame.

The transmit bits b are then interleaved using a random interleaver, where the interleave pattern is generated by a random number generator following a normal distribution, in  $\infty$  order to generate b. When URC coding is employed in conjunction with another coding method, a second interleaving operation is performed after URC encoding using a second random interleaver. The block diagrams of RSC-AFDM and RSC-URC-AFDM are shown in Figs. 1 and 2, respectively.

The interleaved bits  $\overset{\infty}{\boldsymbol{b}}$  are modulated using Phase Shift Keying (PSK) or Quadrature Amplitude Modulation (QAM) to form the AFD transmit signal  $\ddot{\boldsymbol{x}} \in \mathbb{C}^{\ddot{N}\Xi\times 1}$ .  $\ddot{\boldsymbol{x}}$  is then converted to the TD:

$$\mathbf{x}_{\xi} = \mathbf{A}_{\ddot{N}}^{H} \ddot{\mathbf{x}}_{\xi},\tag{1}$$

where  $x_{\xi} \in \mathbb{C}^{\ddot{N} \times 1}$  is the TD transmit signal for the  $\xi$ th transmit block,  $\xi = [0, 1, ..., \Xi - 1]$  is the block index, and  $A_{\ddot{N}}$  is

the  $\ddot{N} \times \ddot{N}$  DAFT, defined as:

$$\mathbf{A}_{\ddot{N}} = \mathbf{\Lambda}_{c_2} \mathbf{F}_{\ddot{N}} \mathbf{\Lambda}_{c_1}, \tag{2}$$

where  $F_{\ddot{N}}$  is the  $\ddot{N} \times \ddot{N}$  DFT,  $c_1$  and  $c_2$  are the chirp parameters 1 and 2, and:

$$\mathbf{\Lambda}_{c} = \operatorname{diag}(e^{-j2\pi c(\ddot{n})^{2}}),\tag{3}$$

where  $\ddot{n} = [0, 1,..., \ddot{N} - 1]$  is the AFDM chirp subcarrier index, and diag(v) generates a square diagonal matrix whose diagonal elements are the elements of v.

Following the conditions outlined in [13],  $c_1$  is set to:

$$c_1 = \frac{2(\ddot{k}_{\text{max}} + k_{\nu}) + 1}{2\ddot{N}},\tag{4}$$

where  $\ddot{k}_{\text{max}}$  is the maximum AFDM Doppler index, defined in (18) further below, and  $k_{\nu}$  is the AFDM guard for fractional indices.

Furthermore,  $c_2$  is set to a small arbitrary irrational number:

$$c_2 = \frac{1}{9^{2\pi}}. (5)$$

Detailed information on the basic concepts of the DAFT and of AFDM can be found in [13].

# **III. CHANNEL AND RECEIVED SIGNAL MODEL**

It is assumed that there is no external interference during transmission, that the CPP for AFDM and the CP for OTFS and OFDM are perfectly removed, and that their lengths are in excess of the maximum channel delay-spread.

The transmitted signal is passed through a typical timevarying and frequency-selective fading channel used in the OTFS literature, as modelled in [38]. The TD representation of this channel for OTFS is:

$$h_{m,n,p,\xi} = \widetilde{h}_p e^{j2\pi \widetilde{k}_p \frac{\xi MN + nM + m - \widetilde{l}_p}{MN}}, \tag{6}$$

where  $j=\sqrt{-1}$ , p=[0,1,...,P-1] is the propagation path index, P is the total number of propagation paths, m=[0,1,...,M-1] denotes the OTFS subcarrier index, M is the number of OTFS subcarriers, n=[0,1,...,N-1] is the OTFS symbol slot index, N is the number of OTFS symbol slots,  $\xi=[0,1,...,\Xi-1]$  is the block index,  $\widetilde{h}_p$  is the fading gain and path loss, while  $\widetilde{l}_p$  and  $\widetilde{k}_p$  are the OTFS delay and Doppler indices associated with the pth propagation path respectively, defined as:

$$\widetilde{l}_p = (\Delta f M) \, \tau_p, \tag{7}$$

$$\widetilde{k}_p = \frac{N}{\Delta f} \nu_p,\tag{8}$$

where  $\Delta f$  is the OTFS subcarrier spacing,  $\tau_p$  is the delay associated with the pth path, and  $\nu_p$  is the Doppler shift associated with the pth path.

This representation assumes integer delay indices, as the delay resolution is assumed to be sufficiently large. The propagation path variables are assumed to be constant over the  $\Xi$  transmission blocks. The equivalent AFDM channel is attained upon substituting MN with  $\ddot{N}$  and  $\Delta f$  with  $\Delta f$ . Hence, the TD representation of the channel for AFDM is:

$$h_{\ddot{n}, p, \xi} = \tilde{h}_p e^{j2\pi \ddot{k}_p \frac{\xi \ddot{N} + \ddot{n} - \ddot{l}_p}{N}}, \tag{9}$$

where  $\ddot{l}_p$  and  $\ddot{k}_p$  are the AFDM delay and Doppler indices associated with the *p*th propagation path respectively:

$$\ddot{l_p} = \left(\ddot{\Delta f} \ddot{N}\right) \tau_p,\tag{10}$$

$$\ddot{k_p} = \frac{v_p}{\ddot{\Lambda}f},\tag{11}$$

where  $\Delta f$  is the AFDM subcarrier spacing.

Therefore, in order to have consistent delay and Doppler indices between (7)-(8) and (10)-(11),  $\ddot{N} = MN$ ,  $\ddot{n} = nM + m$ , and  $\ddot{\Delta}f = \frac{\Delta f}{N}$ .

Each index can be decomposed into its integer- and fractionally-spaced counterparts, e.g.:

$$\widetilde{k}_p = \widetilde{k}_p + \delta \widetilde{k}_p, \tag{12}$$

where the  $\underline{\widetilde{k}_p} = \lfloor \widetilde{k}_p \rceil$  is the integer part of the index,  $\delta \widetilde{k}_p = \widetilde{k}_p - \underline{\widetilde{k}_p}$  is the fractional component, and  $\lfloor \cdot \rceil$  is the rounding function.

Using this notation, the TD channel representations in (6) and (9) can be respectively rewritten as:

$$h_{m,n,p,\xi} = \left(\widetilde{h}_p e^{j2\pi\widetilde{k}_p \frac{nM+m-\widetilde{l}_p}{MN}}\right) e^{j2\pi\delta\widetilde{k}_p \xi}, \tag{13}$$

$$h_{\ddot{n}, p, \xi} = \left(\widetilde{h}_{p} e^{j2\pi \vec{k}_{p} \frac{\ddot{n} - \ddot{l}_{p}}{\ddot{N}}}\right) e^{j2\pi \delta \vec{k}_{p} \xi}.$$
 (14)

It can be readily seen that when the fractional component of the Doppler indices is 0, the channel does not vary with respect to the block index  $\xi$ . When  $\delta k_p$  is non zero, the additional blocks impose a phase shift to the TD channel.

The channel is specifically defined for OTFS and AFDM for explicit clarity, since multiple OTFS and AFDM configurations are considered, as shown in Table 2. When  $\ddot{N}=MN$ ,  $\ddot{n}=nM+m$ , and  $\ddot{\Delta}f=\frac{\Delta f}{N}$ , the TD channels in (13) and (14) of AFDM and OTFS are equal to each other. The equivalence described in this paper between the two waveforms is based on the channel, and therefore on the input-output relationship of the waveforms. The OTFS TD channel representation is also directly applied to OFDM, as OTFS and OFDM utilise the same system parameters.

#### A. PROPAGATION PATH PARAMETER GENERATION

The first path p = 0 is the Line of Sight (LoS) path, while the remaining P - 1 paths are NLoS paths. The fading gain and path loss  $h_p$  is:

$$\widetilde{h}_{p} = \begin{cases}
\sqrt{\frac{\kappa}{\kappa+1}}, & \text{if } p = 0 \\
\sqrt{\frac{1}{(\kappa+1)(P-1)}}\zeta_{p}, & \text{if } p > 0,
\end{cases}$$
(15)

where  $\kappa$  is the Rician K factor, and  $\zeta_p$  is a complex Gaussian random variable with mean  $\mu_h = 0$  and variance  $\sigma_h^2 = 1$ , expressed as  $\mathcal{CN}(\mu_h, \sigma_h^2)$ .

The LoS path has a gain of 1 as the signal propagates directly from the transmitter to the receiver. Hence, it is assumed that only the delay and Doppler shift distort the signal. In the NLoS paths, the signal propagates through a random set of paths, each with their own phase shifts and path losses. As these paths are not known, the random phase shift and path loss are generated using a Gaussian variable, with the overall average power dictated by the Rician K factor.

The delay index  $l_p$  is:

$$l_p = \begin{cases} 0, & \text{if } p = 0\\ \lfloor (D_T - 1)\eta_l \rceil, & \text{if } p > 0, \end{cases}$$
 (16)

where  $D_T$  is the number of delay taps, and  $\eta_l$  is a random variable obeying a uniform distribution between 0 and 1.

The number of delay taps  $D_T$  defines the maximum delay index, and hence the maximum propagation path delay. No pair of propagation paths will have the same delay index, yielding:  $l_{p_1} \neq l_{p_2}$ , where  $p_1 = [0, 1, \dots P - 1]$ ,  $p_2 = [0, 1, \dots P - 1]$ , and  $p_1 \neq p_2$ .

The fractional Doppler index  $k_p$  is:

$$k_p = |2k_{\text{max}}(\eta_k - 0.5)|,$$
 (17)

where  $\eta_k$  is a random variable following a uniform distribution between 0 and 1, and  $k_{\text{max}}$  is the maximum integer Doppler

index, defined as:

$$k_{\text{max}} = \left| \frac{1}{\Delta f} \frac{f_c V}{c_0} \right| = \left| \frac{N}{\Delta f} \frac{f_c V}{c_0} \right|, \tag{18}$$

where V is the velocity of the communication receiver,  $f_c$  is the carrier frequency, and  $c_0$  is the speed of light. The equality holds when equivalent AFDM and OTFS configurations are compared.

# B. CHANNEL MATRIX AND RECEIVED SIGNAL DEFINITION

The TD channel matrix for the  $p^{\text{th}}$  path and block  $\xi$ ,  $\boldsymbol{H}_{p,\xi} \in \mathbb{C}^{\ddot{N} \times \ddot{N}}$ , is formulated as:

$$\boldsymbol{H}_{p,\,\xi}[\ddot{n},\,\lfloor \ddot{n} - \ddot{l}_{p} \rfloor_{\ddot{N}}] = h_{\ddot{n},\,p,\,\xi},\tag{19}$$

where  $\lfloor \cdot \rfloor_{\ddot{N}}$  is the modulo  $\ddot{N}$  operator.

The TD channel matrix for all paths for the block  $\xi$ ,  $H_{\xi} \in \mathbb{C}^{\ddot{N} \times \ddot{N}}$ , is the superposition of the individual path channel matrices, formulated as:

$$H_{\xi} = \sum_{p=0}^{P-1} H_{p,\,\xi}.$$
 (20)

For OTFS, the  $h_{\ddot{n}, p, \xi}$  is replaced by  $h_{m, n, p, \xi}$ , with nM + m instead of  $\ddot{n}$ ,  $\ddot{N}$  substituted by MN, and the OTFS delay and Doppler indices utilised.

The TD received signal for block  $\xi, y_{\xi} \in \mathbb{C}^{\hat{N} \times 1}$ , is:

$$\mathbf{y}_{\xi} = \mathbf{H}_{\xi} \mathbf{x}_{\xi} + \mathbf{z}_{\xi},\tag{21}$$

where  $z_{\xi}$  is the complex-valued Additive White Gaussian Noise (AWGN) for block  $\xi$ , with mean  $\mu_z = 0$  and variance  $N_0$ , expressed as  $\mathcal{CN}(\mu_z, N_0)$ , and  $N_0$  is the noise power.

The AFD received signal for block  $\xi, \ddot{y}_{\xi} \in \mathbb{C}^{N \times 1}$ , is:

$$\ddot{\mathbf{y}}_{\xi} = \mathbf{A}_{\ddot{N}} \mathbf{y}_{\xi} = \mathbf{A}_{\ddot{N}} \mathbf{H}_{\xi} \mathbf{A}_{\ddot{N}}^{H} \ddot{\mathbf{x}}_{\xi} + \mathbf{A}_{\ddot{N}} \mathbf{z}_{\xi},$$

$$\ddot{\mathbf{y}}_{\xi} = \ddot{\mathbf{H}}_{\xi} \ddot{\mathbf{x}}_{\xi} + \mathbf{A}_{\ddot{N}} \mathbf{z}_{\xi},$$
(22)

where  $\ddot{H}_{\xi}$  is the AFD equivalent channel:

$$\ddot{\boldsymbol{H}}_{\xi} = \boldsymbol{A}_{\ddot{N}} \boldsymbol{H}_{\xi} \boldsymbol{A}_{\ddot{N}}^{H}. \tag{23}$$

### **IV. SOFT-MMSE DETECTION**

Soft-MMSE equalisation [39] is applied at the receiver, with perfect channel estimation assumed. Due to the interleaving applied to the coded bits, the channel decoder's *a posteriori* Log-Likelihood Ratios (LLRs)  $\mathcal{L}^{\rho,\delta}$  are interleaved to generate the soft-MMSE *a priori* LLRs  $\mathcal{L}^{\alpha,\mu}$ .

For each transmit block  $\xi$ , a transmit symbol estimate  $\varepsilon\{\ddot{x}_{\xi}\}$  is formulated using the soft-MMSE *a priori* LLRs  $\mathcal{L}_{\xi}^{\alpha,\mu}$  for the  $\xi^{\text{th}}$  transmit block as:

$$\varepsilon\{\ddot{\mathbf{x}}_{\xi}[\ddot{n}]\} = \sum_{\gamma=0}^{\Gamma-1} s_{\gamma} \mathcal{P}\left(\ddot{\mathbf{x}}_{\xi}[\ddot{n}] = s_{\gamma}\right),\,$$

$$= \sum_{\gamma=0}^{\Gamma-1} s_{\gamma} \frac{\exp\left(\sum_{\beta=0}^{B_{S}-1} b_{\beta}^{\gamma} \mathcal{L}_{\xi}^{\alpha,\mu} [\ddot{n}B_{S} + \beta]\right)}{\prod_{\beta=0}^{B_{S}-1} \left(1 + \exp\left(\mathcal{L}_{\xi}^{\alpha,\mu} [\ddot{n}B_{S} + \beta]\right)\right)},$$
(24)

where  $\mathcal{P}(a=b)$  denotes the probability of a=b,  $s_{\gamma}$  is the modulated symbol corresponding to the integer value  $\gamma$ ,  $\gamma=[0, 1,..., \Gamma-1]$  is the modulation index,  $\beta=[0, 1,..., B_S-1]$  is the index of bits in a symbol, and  $\exp(\cdot)$  is the natural exponential function.

A diagonal matrix E of the squared magnitude of  $\varepsilon\{\ddot{x}_{\xi}\}$  is then generated as:

$$E = \operatorname{diag}\left(\varepsilon\{\ddot{\mathbf{x}}_{\xi}\} \otimes \varepsilon\{\ddot{\mathbf{x}}_{\xi}\}^{*}\right), \tag{25}$$

where  $\otimes$  is the element-wise multiplication, and  $(\cdot)^*$  is the complex conjugate operation.

The AFDM MMSE matrix  $\ddot{G}_{\xi}$  for the  $\xi^{\text{th}}$  transmit block is:

$$\ddot{\boldsymbol{G}}_{\xi} = \left(\ddot{\boldsymbol{H}}_{\xi}^{*} \left(\boldsymbol{R}_{SX} + \boldsymbol{E}\right) \ddot{\boldsymbol{H}}_{\xi}^{T} + N_{0} \boldsymbol{I}_{\ddot{N} \times \ddot{N}}\right)^{-1} \ddot{\boldsymbol{H}}_{\xi}^{*}, \tag{26}$$

where  $(\cdot)^T$  is the transpose operation,  $I_{\ddot{N}\times\ddot{N}}$  is the  $\ddot{N}\times\ddot{N}$  identity matrix, and  $R_{SX}$  is the covariance matrix of the transmit symbols, which is set to  $I_{\ddot{N}\times\ddot{N}}$ , since the average transmit symbols power is normalised to 1.

The soft-MMSE transmit signal estimate  $\mathbf{x}^{\mu}$  is expressed:

$$\overset{\mu}{\mathbf{x}}[\ddot{n}] = \left( \left( \ddot{\mathbf{y}}_{\xi} \right)^T \ddot{\mathbf{g}}_{\xi, \ddot{n}} - \iota_{\xi, \ddot{n}} \right) \frac{\binom{\mu}{h_{\xi, \ddot{n}}}^*}{|h_{\xi, \ddot{n}}|^2}, \tag{27}$$

where  $|\cdot|$  is the magnitude operator,  $\ddot{\mathbf{g}}_{\xi,\ddot{n}}$  is the  $\ddot{n}^{\text{th}}$  column of  $\ddot{\mathbf{G}}_{\xi}$ ,  $\iota_{\xi,\ddot{n}}$  is the interference imposed upon the  $\ddot{n}^{\text{th}}$  symbol by the other  $\ddot{N}-1$  symbols in the  $\xi^{\text{th}}$  transmit block, and  $h_{\xi,\ddot{n}}$  is:

$$\overset{\mu}{h_{\xi,\ddot{n}}} = \left( \ddot{\boldsymbol{h}}_{\xi,\ddot{n}} \right)^T \ddot{\boldsymbol{g}}_{\xi,\ddot{n}}.$$
(28)

The interference imposed upon the  $\ddot{n}^{\text{th}}$  symbol by the other  $\ddot{N}-1$  symbols in the  $\xi^{\text{th}}$  transmit block  $\iota_{\xi,\ddot{n}}$  is:

$$\iota_{\xi,\ddot{n}} = \sum_{\ddot{n}_2 = 0, \ddot{n}_2 \neq \ddot{n}}^{\ddot{N} - 1} \varepsilon \{ \ddot{\boldsymbol{x}}_{\xi} [\ddot{n}_2] \} \left( \ddot{\boldsymbol{h}}_{\xi, \ddot{n}_2} \right)^T \ddot{\boldsymbol{g}}_{\xi, \ddot{n}}. \tag{29}$$

The equivalent soft-MMSE AWGN noise power  $N_{0,\xi}$  for each symbol is expressed as:

$$\overset{\mu}{N}_{0,\xi}[\ddot{n}] = \frac{1}{\overset{\mu}{|h_{\xi,\ddot{n}}|}} + (\boldsymbol{E}[\ddot{n},\ddot{n}] - 1).$$
(30)

The approximate maximum probability metric  $d_{m,\gamma}^{\mu}$  describing the probability of the transmit symbol  $\ddot{x}[m]^{\mu}$  being  $s_{\gamma}$  can then be generated using  $x[m]^{\mu}$  and  $N_{0,\xi}$ :

$$d_{m,\gamma}^{\mu} = -\frac{\left|\mathbf{x}[m] - s_{\gamma}\right|^{2}}{N_{0}[m]} + \sum_{\beta=0}^{B_{S}-1} b_{\beta}^{\gamma} \mathcal{L}_{\xi}^{\alpha,\mu}[\ddot{b}], \quad (31)$$

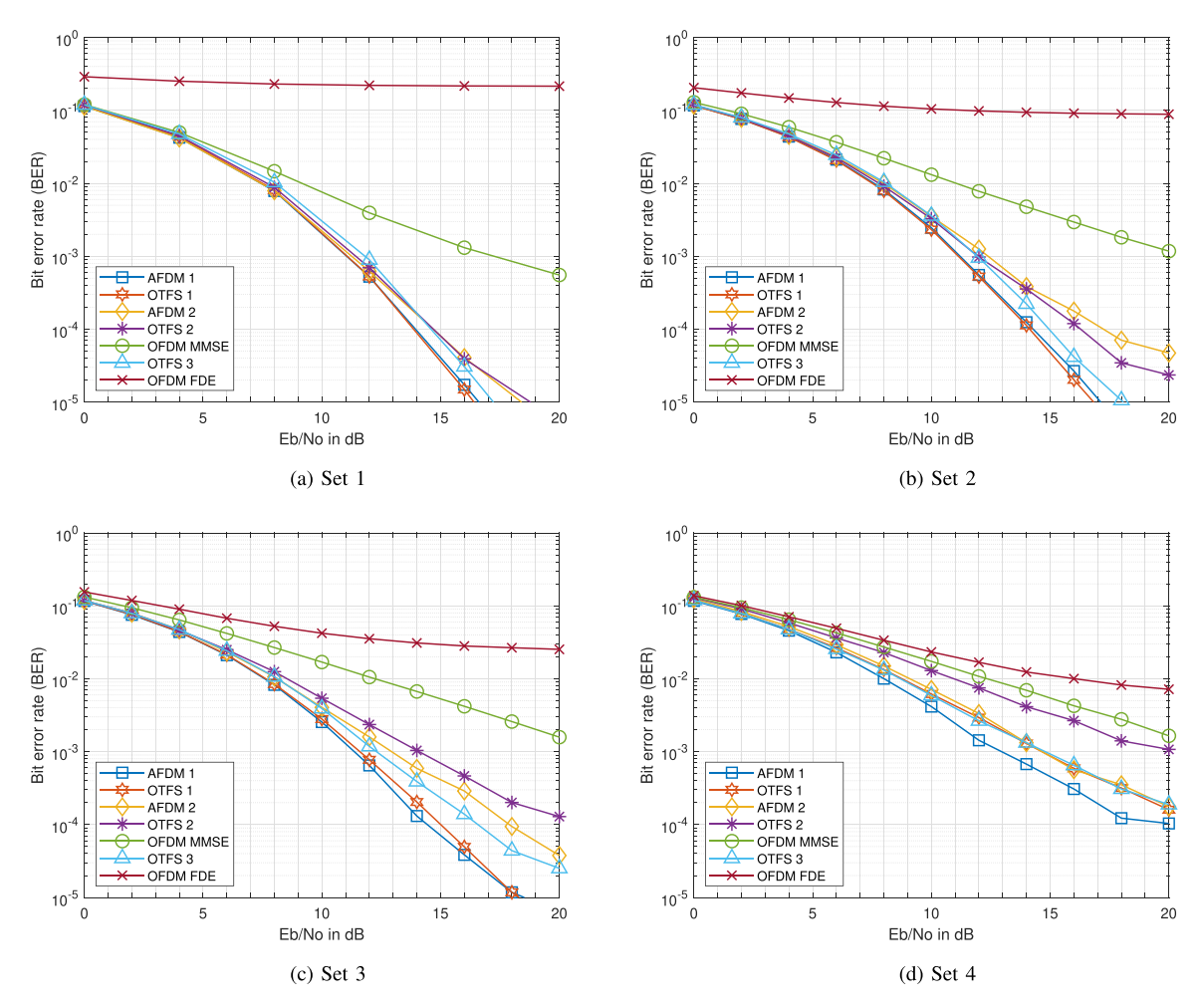


FIGURE 3. BER of uncoded BPSK AFDM 1 and 2, OFDM, and OTFS 1, 2 and 3

TABLE 3. Lookup Table for the Jacobian Algorithm

| Value of $ d_1 - d_2 $       | Value of $\Theta( d_1 - d_2 )$ |
|------------------------------|--------------------------------|
| $ d_1 - d_2  > 3.7$          | 0                              |
| $2.25 <  d_1 - d_2  \le 3.7$ | 0.05                           |
| $1.5 <  d_1 - d_2  \le 2.25$ | 0.15                           |
| $1.05 <  d_1 - d_2  \le 1.5$ | 0.25                           |
| $0.7 <  d_1 - d_2  \le 1.05$ | 0.35                           |
| $0.43 <  d_1 - d_2  \le 0.7$ | 0.45                           |
| $0.2 <  d_1 - d_2  \le 0.43$ | 0.55                           |
| $ d_1 - d_2  \le 0.2$        | 0.65                           |

where  $\ddot{b} = [0, 1, ..., \ddot{N}B_S - 1]$  is the bit index within the transmit block  $\xi$ ,  $\overset{\mu}{m} = \lfloor \frac{\ddot{b}}{B_S} \rfloor$ , and  $\lfloor \cdot \rfloor$  is the floor function.

The soft-MMSE a posteriori LLRs  $\mathcal{L}_{\xi}^{\rho,\mu}$  for the  $\xi^{\text{th}}$  transmit block are then calculated using the Approx-Log-MAP algorithm from [39], [40]:

$$\mathcal{L}_{\xi}^{\rho,\mu}[\ddot{b}] = \operatorname{jac}\begin{pmatrix} \mu \\ d_{m,\gamma} \end{pmatrix} - \operatorname{jac}\begin{pmatrix} \mu \\ d_{m,\gamma} \end{pmatrix}, \qquad (32)$$

$$s_{\gamma} \in \mathcal{S}_{b_{\xi}=1} \qquad s_{\gamma} \in \mathcal{S}_{b_{\xi}=0}$$

where  $jac(\cdot)$  is the Jacobian function:

$$jac (d_1, d_2) = max (d_1, d_2) + \Theta(|d_1 - d_2|), \qquad (33)$$

where max is the maximum function that returns the highest value, and  $\Theta(|d_1-d_2|)$  is an additional term whose value is specified by Table 3 [41], [42]. The soft-MMSE algorithm outputs the *a posteriori* LLRs for the  $\Xi$  transmit blocks  $\mathcal{L}^{\rho,\mu} \in \mathbb{R}^{R_c B_s \ddot{N} \Xi \times 1}$ . The *a posteriori* LLRs  $\mathcal{L}^{\rho,\mu}$  are then deinterleaved to produce the channel decoder's *a priori* LLRs  $\mathcal{L}^{\alpha,\delta}$ , which are then passed to the RSC decoder when RSC coding is employed, or to the URC decoder when RSC-URC coding is utilised, as shown in Figs. 1 and 2, respectively. For AFDM, the *a posteriori* LLRs are  $\ddot{\mathcal{L}}^{\rho,\mu} \in \mathbb{R}^{R_c B_s \ddot{N} \Xi \times 1}$ , whereas for OTFS, they are  $\mathcal{L}^{\rho,\mu} \in \mathbb{R}^{R_c B_s MN \Xi \times 1}$ . The soft-MMSE method presented is used for AFDM, OTFS, and OFDM, as it is independent of the waveform or signal domain.

# **V. SIMULATION RESULTS**

The simulation parameters are shown in Table 4. The number of subcarriers refers to OFDM-type subcarriers for OFDM and OTFS, and to chirp subcarriers for AFDM. Different random interleavers are generated for each frame. The same

**TABLE 4. Simulation Parameter Values** 

| Parameter                                  | OFDM    | AFDM 1              | OTFS 1  | AFDM 2  | OTFS 2  | OTFS 3              |  |  |  |  |
|--|---------|---------------------|---------|---------|---------|---------------------|--|--|--|--|
| Modulation order $\Gamma$                  |         | l .                 | 2       | }       |         | l .                 |  |  |  |  |
| Number of propagation paths P              | 4       |                     |         |         |         |                     |  |  |  |  |
| Number of delay taps $D_T$                 |         |                     | 5       |         |         |                     |  |  |  |  |
| Communication receiver velocity $V$        | 150 m/s |                     |         |         |         |                     |  |  |  |  |
| Rician K factor $\kappa$                   |         |                     | 0 0     | lΒ      |         |                     |  |  |  |  |
| Carrier frequency $f_c$                    |         |                     | 38.5    | GHz     |         |                     |  |  |  |  |
| Maximum propagation delay $	au_{max}$      |         |                     | 10.41   | 67 μs   |         |                     |  |  |  |  |
| AFDM guard for fractional indices $k_{ u}$ | N/A     | 1                   | N/A     | 1       | N/A     | N/A                 |  |  |  |  |
|  |         | Set 1               |         |         |         |                     |  |  |  |  |
| Number of subcarriers                      | 32      | 512                 | 32      | 32      | 8       | 32                  |  |  |  |  |
| Number of symbol slots                     | 16      | N/A                 | 16      | N/A     | 4       | 16                  |  |  |  |  |
| Subcarrier spacing                         | 15 kHz  | $\frac{15}{16}$ kHz | 15 kHz  | 15 kHz  | 60 kHz  | $\frac{15}{16}$ kHz |  |  |  |  |
|  | Set 2   |                     |         |         |         |                     |  |  |  |  |
| Number of subcarriers                      | 16      | 128                 | 16      | 16      | 8       | 16                  |  |  |  |  |
| Number of symbol slots                     | 8       | N/A                 | 8       | N/A     | 2       | 8                   |  |  |  |  |
| Subcarrier spacing                         | 30 kHz  | $\frac{15}{4}$ kHz  | 30 kHz  | 30 kHz  | 60 kHz  | $\frac{15}{4}$ kHz  |  |  |  |  |
|  |         | Set 3               |         |         |         |                     |  |  |  |  |
| Number of subcarriers                      | 8       | 32                  | 8       | 8       | 4       | 8                   |  |  |  |  |
| Number of symbol slots                     | 4       | N/A                 | 4       | N/A     | 2       | 4                   |  |  |  |  |
| Subcarrier spacing                         | 60 kHz  | 15 kHz              | 60 kHz  | 60 kHz  | 120 kHz | 15 kHz              |  |  |  |  |
| Set 4                                      |         |                     |         |         |         |                     |  |  |  |  |
| Number of subcarriers                      | 4       | 8                   | 4       | 4       | 2       | 4                   |  |  |  |  |
| Number of symbol slots                     | 2       | N/A                 | 2       | N/A     | 2       | 2                   |  |  |  |  |
| Subcarrier spacing                         | 120 kHz | 60 kHz              | 120 kHz | 120 kHz | 240 kHz | 60 kHz              |  |  |  |  |

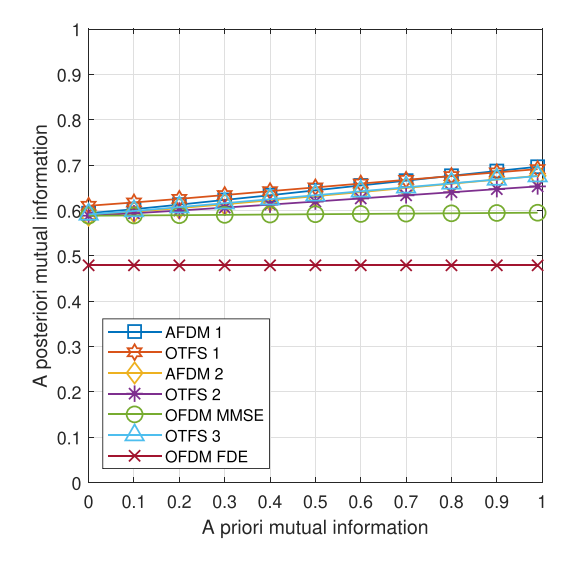


FIGURE 4. EXIT chart of Set 4 soft-MMSE BPSK AFDM 1 and 2, OFDM, and OTFS 1 and 2 for 0 dB Eb/NO.

interleaver is utilised across transmission blocks within a frame, and the interleaver length is 10 000 bits.

The five configurations outlined in Table 2 are characterised by simulations. OFDM is configured to match OTFS 1, with multiple symbol slots. AFDM 1 is equivalent to OTFS 1, hence it possesses a smaller subcarrier spacing than OFDM

and OTFS 1, to ensure that the same frequency resources are utilised. The duration of AFDM 2 is equal to that of a single OFDM symbol, and has the same subcarrier spacing as OFDM. OTFS 2 is the configuration that is equivalent to AFDM 2. OTFS 3 has the same matrix dimension and subcarrier spacing as AFDM 1, hence it has a lower bandwidth. OTFS 3 is included since some references utilise this OTFS configuration to compare with AFDM.

Four parameter value groups are investigated, named Set 1, 2, 3, and 4. The matrix dimensions of OFDM, OTFS 1, and AFDM 1 are divided by 4 every time the Set index is increased. The values of the base variables defined in Table 2 are, for each Set:

- Set 1: M = 32, N = 16,  $\Delta f = 15$  kHz.
- Set 2: M = 16, N = 8,  $\Delta f = 30$  kHz.
- Set 3: M = 8, N = 4,  $\Delta f = 60$  kHz.
- Set 4: M = 4, N = 2,  $\Delta f = 120$  kHz.

# A. UNCODED BER

The BERs of uncoded Binary Phase Shift Keying (BPSK) AFDM 1 and 2, OTFS 1, 2, and 3, and OFDM utilising hard-MMSE are shown in Fig. 3. The BER of OFDM using single tap Frequency Domain (FD) equalisation, denoted as "FDE", is also shown. Hard-MMSE refers to the MMSE equalisation that outputs bit estimates (hard values), as opposed to LLRs (soft values). For Set 1, the BERs of the AFDM and OTFS

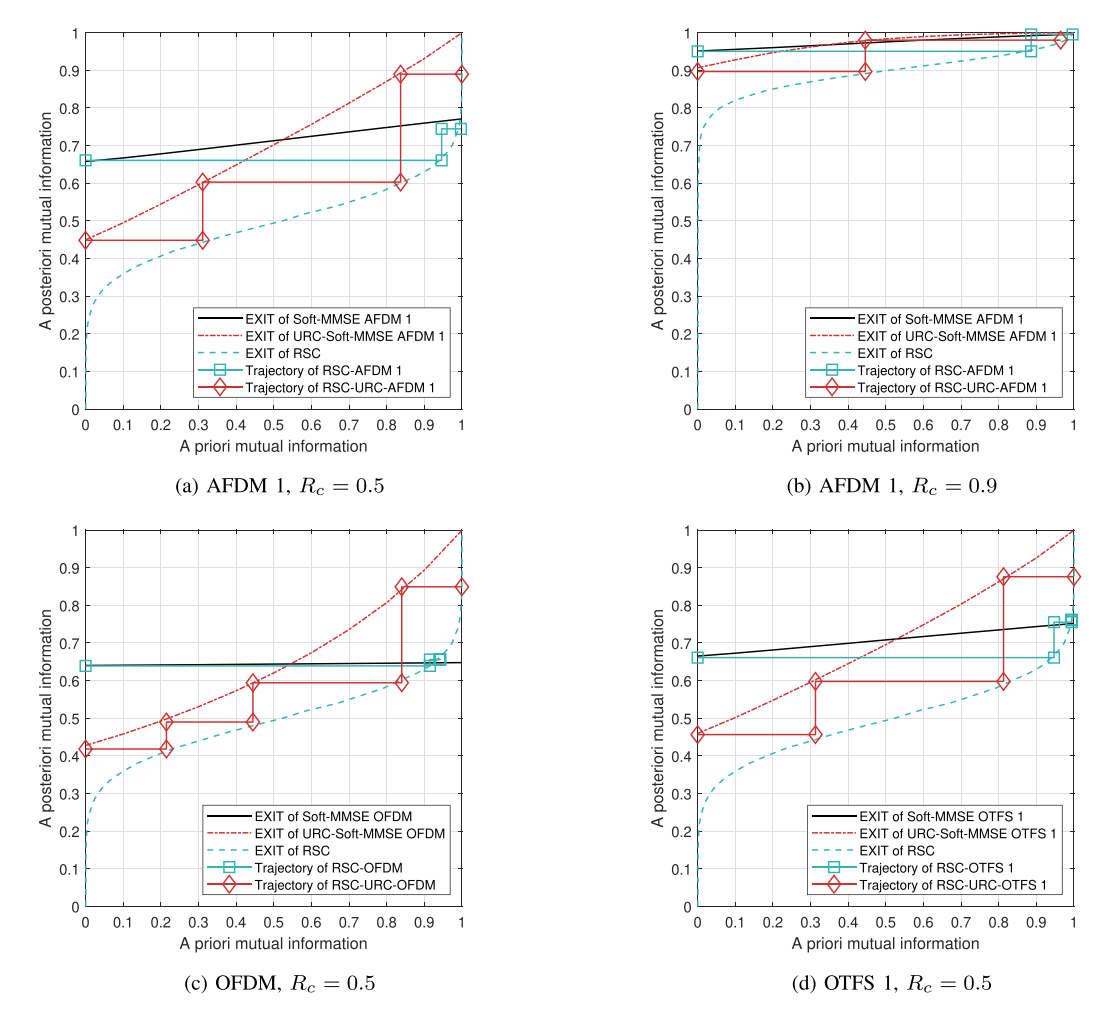


FIGURE 5. EXIT chart and trajectory of Set 4 RSC- (square) and RSC-URC-coded (diamond) BPSK AFDM 1, OFDM, and OTFS 1 for 4 dB Eb/NO

configurations are similar to each other. The BER of hard-MMSE OFDM is higher than that of AFDM and OTFS, with the BER of "FDE" OFDM remaining above 0.3 for the Energy per bit over Noise power (Eb/NO) range considered.

When the Set index is increased, the dimension of the configurations is reduced, and the BERs of the AFDM configurations do not increase to the same extent as the BERs of their OTFS counterparts at high Eb/NO. AFDM 1 is the counterpart to OTFS 1, and AFDM 2 is the counterpart to OTFS 2. OTFS 3 has no direct counterpart, and it is included to illustrate how a non-equivalent configuration may result in an unfair comparison between OTFS and AFDM. OTFS 3 has the same subcarrier spacing and dimension as AFDM 1, which results in OTFS 3 possessing a smaller bandwidth than AFDM 1.

It can be observed from Fig. 3 that for Set 1, associated with the largest matrix dimension, AFDM 1 and OTFS 1 exhibit a similar BER, while the BER of AFDM 2 is comparable to that of OTFS 2. However, as the matrix dimension is reduced from that of Set 1 to Set 4, the AFDM configurations gradually start to outperform their OTFS counterparts. This is because to AFDM's diversity gain only presenting a

significant advantage when the codeword differences are small, for small matrix dimensions. Therefore, Set 4 is utilised for the majority of the following results, as it is the parameter Set for which AFDM exhibits the most substantial BER improvement over OTFS.

### **B. EXIT CHART ANALYSIS**

The EXIT charts of Set 4 soft-MMSE BPSK AFDM 1 and 2, OTFS 1, 2, and 3, and OFDM for 0 dB Eb/NO are shown in Fig. 4. As expected, the *a posteriori* mutual information is increased when the *a priori* mutual information is increased. This demonstrates that the soft-MMSE method is capable of improving the performance compared to hard MMSE. The EXIT curves of AFDM 1 and OTFS 1 are similar to each other, indicating a similar performance. The EXIT curve of AFDM 2 has a steeper gradient than that of OTFS 2, which suggests that AFDM 2 has a superior detection capability to OTFS 2. The EXIT curve of soft-MMSE OFDM is at a higher ordinate value than that of hard-MMSE OFDM, but maintains the same 0 gradient, which indicates that soft-MMSE OFDM cannot provide an iteration gain. The EXIT curve of soft-MMSE OFDM is also at a lower ordinate value than those

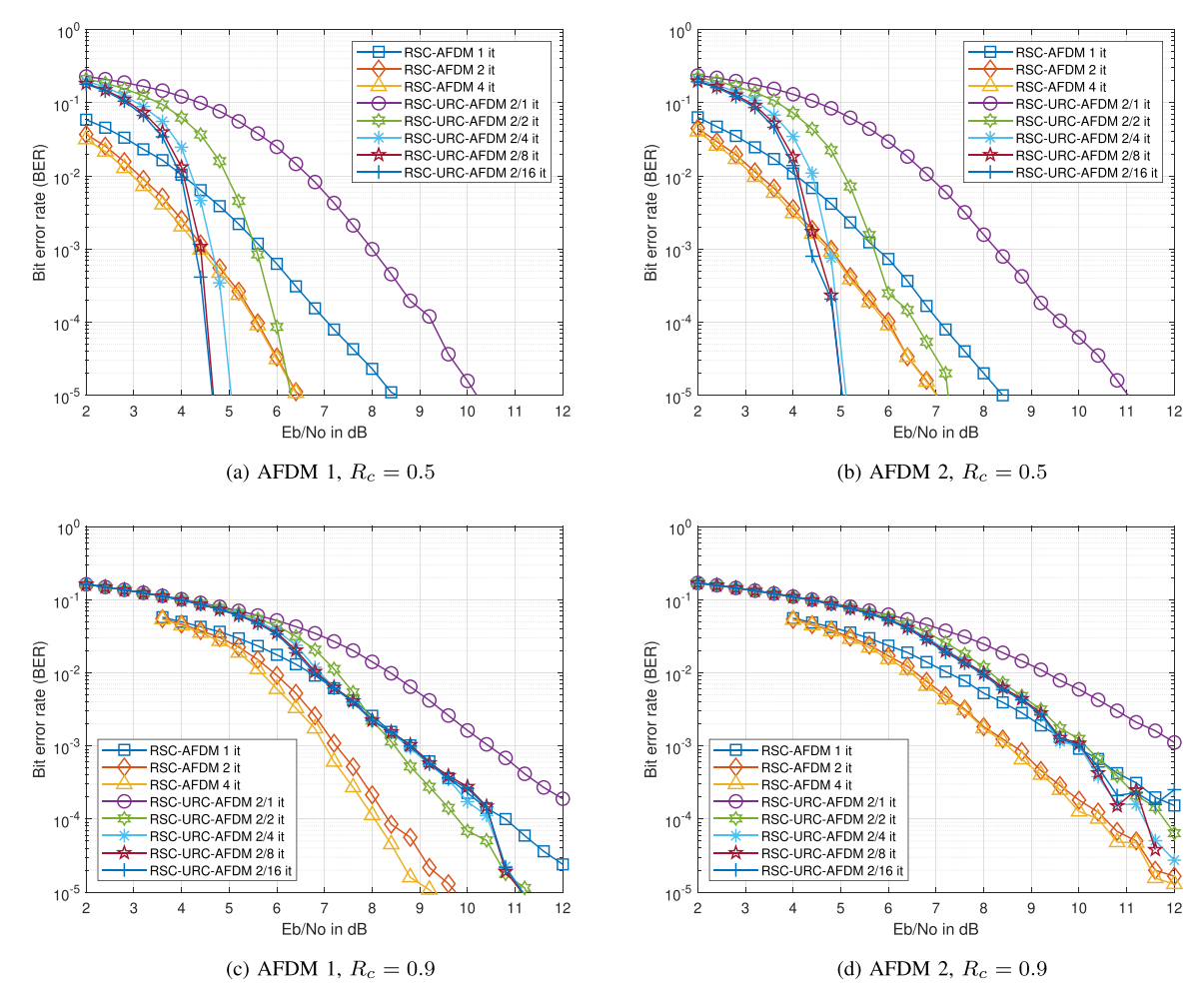


FIGURE 6. BER of Set 4 RSC- and RSC-URC-coded BPSK AFDM 1 and 2

of AFDM and OTFS. The lack of gradient in the soft-MMSE OFDM EXIT curve is due to the lack of correlation between the OFDM subcarriers, when no AFDM or OTFS precoding is implemented.

The EXIT charts and trajectories of Set 4 RSC- and RSC-URC-coded BPSK AFDM 1, OTFS 1 and OFDM for soft-MMSE are shown in Fig. 5, for 4 dB Eb/NO. The trajectories of AFDM 1 and OTFS 1 are similar, which reflects the general trend of approximately similar performance between AFDM and OTFS. Due to the flat EXIT chart of soft-MMSE OFDM, there is little iterative gain is attained for RSC coding.

The trajectories of RSC coding reach their end points in 1 or 2 iterations for AFDM 1 and OTFS 1. At a coding rate of 0.9, the minimum *a posteriori* mutual information is 0.9, which only leaves room for modest iteration gain. Hence, the RSC coded AFDM 1 and OTFS 1 trajectories approach the ideal (1, 1) point of perfect convergence.

When URC is harnessed, the EXIT chart performance of soft-MMSE is improved for all three waveforms for  $R_c = 0.5$ , which leads to a higher iterative gain for RSC coding, as the trajectory end point is closer to the ideal (1, 1) point. This is a benefit of the URC increasing the open tunnel. A greater

number of iterations is required to reach the (1, 1) point when URC is employed, but this phenomenon no longer persists at higher coding rates, as shown in Fig. 5(b) for  $R_c = 0.9$ , as the initial *a posteriori* mutual information is very high (0.9). The performance of RSC-URC-OFDM remains lower than that of RSC-URC-AFDM 1 and RSC-URC-OTFS 1.

### C. COMPARISON OF RSC AND RSC-URC AFDM

The BERs of Set 4 RSC- and RSC-URC-coded BPSK AFDM 1 and 2 are shown in Fig. 6, for  $R_c = 0.5$  and 0.9. "RSC-AFDM 1 it" refers to RSC-AFDM relying on a single iteration, and "RSC-URC-AFDM 2/4 it" refers to RSC-URC-AFDM having 2 inner and 4 outer iterations. For RSC-URC coding, the inner iterations are between URC decoding and soft-MMSE equalisation. The outer iterations are between the RSC decoder and the combined URC-equaliser block.

As expected, increasing the coding rate increases the BER for both AFDM configurations and for both coding methods. The BER of RSC-AFDM 1 is lower than that of RSC-AFDM 2 at high Eb/NO and for a sufficiently high number of iterations, following the trend for uncoded hard-MMSE AFDM simulated with the Set 4 variable values. The BER difference is accentuated when the coding rate is increased, as

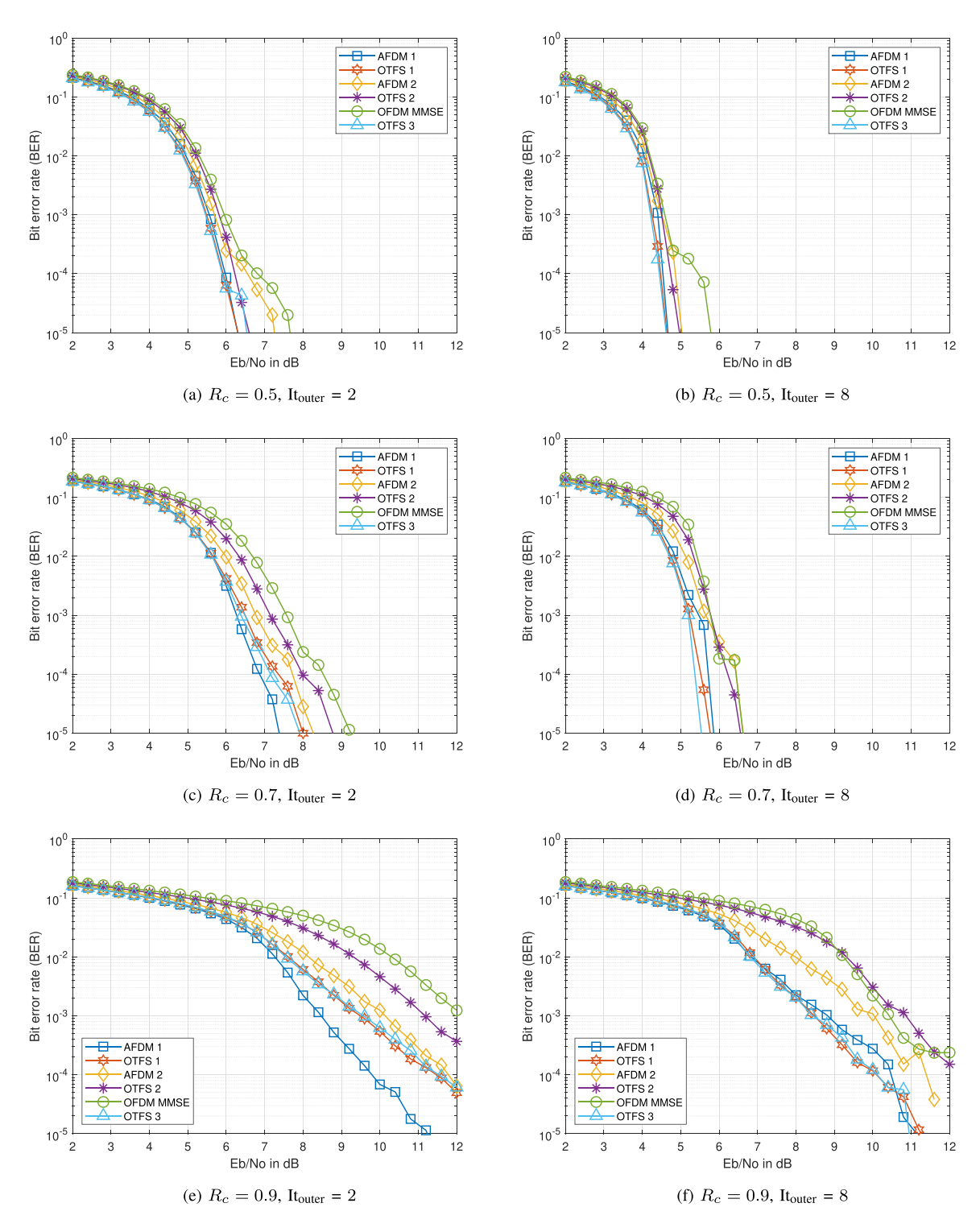


FIGURE 7. BER of Set 4 RSC- and RSC-URC-coded BPSK AFDM 1 and 2, OFDM, and OTFS 1, 2, and 3 for It<sub>inner</sub> = 2

fewer errors can be corrected at high coding rates. The BER of RSC-URC-AFDM 1 is lower than that of AFDM 2 for both coding rates and for the specific number of inner and outer iterations considered.

For RSC coding, increasing the number of iterations from 1 to 2 drastically reduces the BER for both coding rates. By contrast, increasing the number of iterations from 2 to 4 no

longer significantly improves the BER for a coding rate of 0.5, but slightly lowers it for a coding rate of 0.9. This result is consistent with the EXIT chart based prediction, where the trajectory end point is reached within a low number of iterations. The drastic BER reduction of RSC coding as the number of iterations increases is indeed expected as an explicit benefit of having iteratively improved extrinsic LLRs.

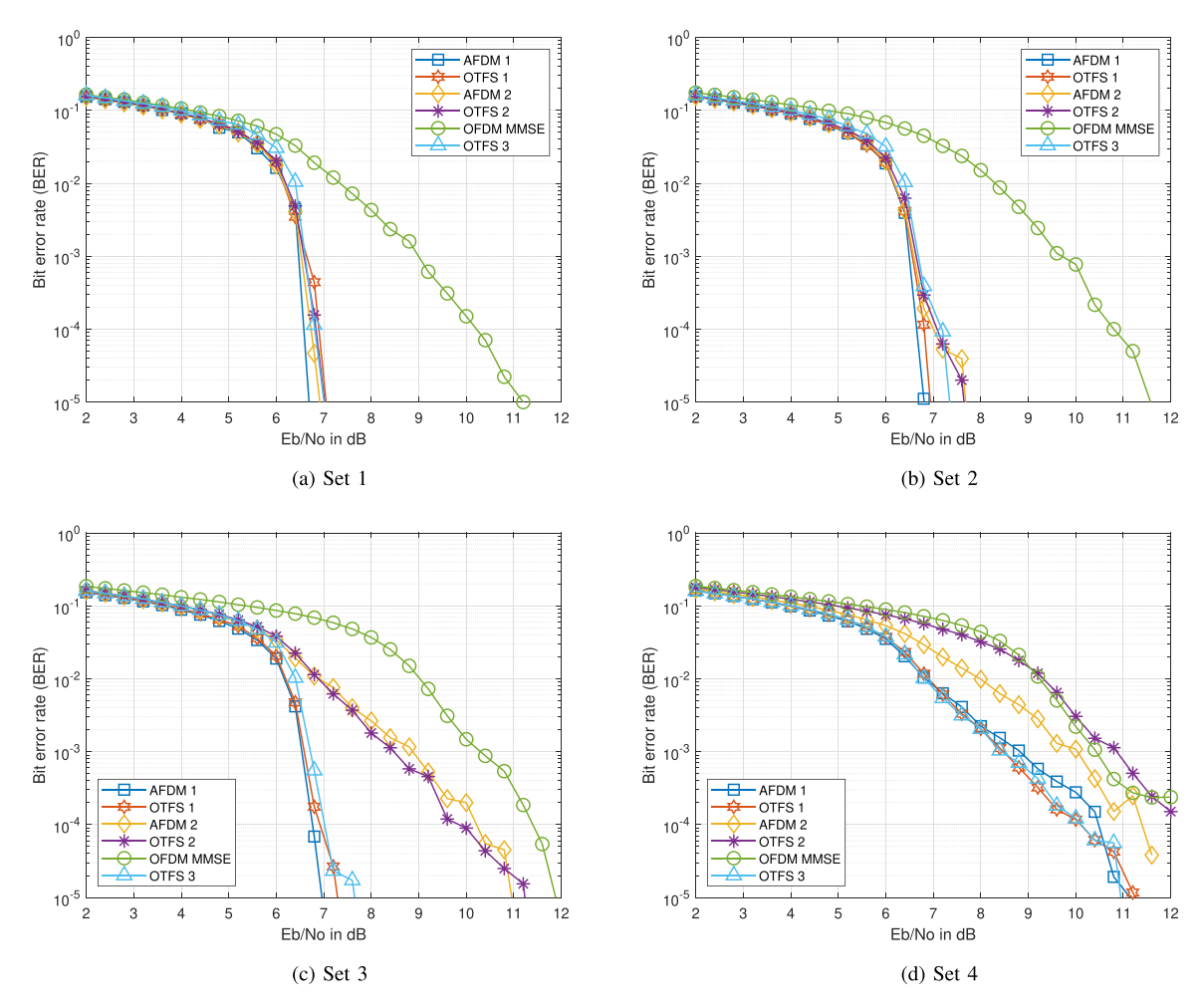


FIGURE 8. BER of Set 1, 2, 3, and 4 RSC-URC-coded BPSK AFDM 1 and 2, OFDM, and OTFS 1, 2 and 3 for R<sub>c</sub> = 0.9 and It<sub>inner</sub> = 2 and It<sub>outer</sub> = 8 iterations

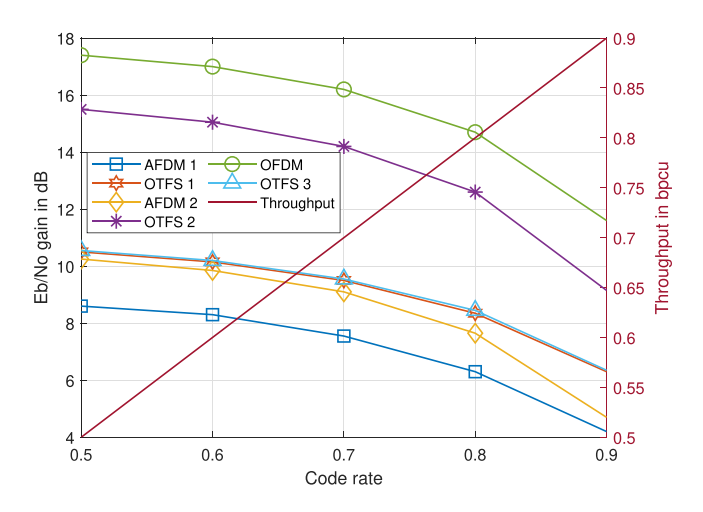


FIGURE 9. Eb/NO gains of Set 4 RSC-URC-coded BPSK AFDM 1 and 2, OFDM, and OTFS 1 and 2 relative to uncoded transmission for  $R_{\rm c}=0.5$  to 0.9 and It<sub>inner</sub> = 2 and It<sub>outer</sub> = 8 iterations at a BER of  $10^{-3}$ .

The BER of RSC-URC coding is higher for both coding rates than that of stand-alone RSC coding when a similar complexity is considered, which is a plausible reflection of the fact that RSC-URC can only improve the BER at an

increased complexity. To elaborate, at a coding rate of 0.5, the BER of RSC-URC coding decreases as the number of outer iterations is increased up to 8. Further increase in the number of iterations does not significantly improve the BER performance. Again, RSC-URC is capable of outperforming RSC coding at the lower coding rates, but only at higher numbers of iterations. This is consistent with the EXIT chart predictions, where the trajectory end point for RSC-URC is only reached at a higher number of iterations than for RSC coding, but it is closer to the ideal (1, 1) point. At a coding rate of 0.9, the BER of RSC-URC is higher than that of RSC coding, even when a higher number of outer iterations is utilised. This is also shown in the EXIT chart results, where the addition of URC does not significantly impact the EXIT curve gradient of soft-MMSE equalisation at this coding rate. At small matrix dimensions, high code rates and many outer iterations, the BER of RSC-URC coding becomes unstable at high Eb/NO, as shown in Fig. 6(d).

#### D. BER OF RSC-URC CODED OFDM, AFDM, AND OTFS

The BERs of Set 4 RSC-URC-coded BPSK AFDM 1 and 2, OFDM, and OTFS 1, 2, and 3 are shown in Fig. 7, for coding rates of 0.5, 0.7, and 0.9, and for  $It_{inner} = 2$ , and  $It_{outer} = 2$  and

| Set index | AFDM 1 | OTFS 1 | AFDM 2 | OTFS 2 | OTFS 3 | OFDM MMSE |
|-----------|--------|--------|--------|--------|--------|-----------|
| Set 1     | 6.6    | 6.9    | 6.7    | 6.85   | 6.8    | 10.2      |
| Set 2     | 6.7    | 6.8    | 7      | 7      | 7.2    | 10.8      |

10.2

11.4

TABLE 5. Eb/NO in dB At Which a BER of  $10^{-4}$  Is Achieved for RSC-URC Coding,  $R_c = 0.9$ , 2 Inner Iterations, and 8 Outer Iterations

6.9

10

6.8

10.2

8. For all coding rates and number of outer iterations, OFDM has the highest BER trend.

Set 3

Set 4

For  $R_c = 0.5$ , the BER of AFDM 1, OTFS 1 and OTFS 3 are similar to each other, with OTFS 2, AFDM 2, and OFDM exhibiting a higher BER. For It<sub>outer</sub> = 2, increasing  $R_c$  increases the relative BER difference of the configurations. AFDM 1 has the lowest BER, followed by OTFS 1 and 3, then AFDM 2, OTFS 2, and OFDM. Recall that AFDM 1, OTFS 1, and OTFS 3 have the larger matrix dimensions, hence they combat the effect of the channel and AWGN better, albeit at the expense of increased complexity. Furthermore, AFDM 2 and OTFS 2 have lower matrix dimensions, which leads to a higher BER, but a lower complexity. At the high velocity considered, the subcarrier orthogonality of OFDM is partially compromised, leading to higher BERs. These trends follow those observed for uncoded transmissions in Fig. 3(d).

When the number of outer iterations is increased to  $It_{outer} = 8$ , the relative difference in BER between the configurations is reduced. The BER trends of AFDM 1, OTFS 1, and OTFS 3 are similar to each other. Observe that AFDM 2, OTFS 2, and OFDM have similar BER trends to each other for  $R_c = 0.5$  and 0.7, with a higher BER than AFDM 1, OTFS 1, and OTFS 3. At  $R_c = 0.9$ , the BER of AFDM 2 is higher than that of AFDM 1, OTFS 1, and OTFS 3, but lower than that of OTFS 2 and OFDM. This is an explicit benefit of AFDM's higher degrees of freedom than those of OTFS and OFDM, which effects the BER performance at low matrix dimensions.

# E. EFFECT OF THE MATRIX DIMENSIONS ON THE BER OF RSC-URC CODED OFDM, AFDM, AND OTFS

The BERs of RSC-URC-coded BPSK AFDM 1 and 2, OFDM, and OTFS 1, 2 and 3 are shown in Fig. 8 for  $R_c = 0.9$  and  $It_{inner} = 2$  and  $It_{outer} = 8$  iterations, for the variable values of Set 1, 2, 3 and 4. When the Set index is reduced, the dimension of the system configurations is increased. As the matrix dimensions are increased, the BER trends of the AFDM and OTFS configurations converge, since the effect of the matrix dimensions is diminished.

# F. EB/NO GAIN OF RSC-URC CODING RELATIVE TO UNCODED TRANSMISSION

The Eb/NO gains of Set 4 RSC-URC-coded BPSK AFDM 1 and 2, OFDM, and OTFS 1 and 2 relative to uncoded transmission for  $R_c = 0.5$  to 0.9 and It<sub>inner</sub> = 2 and It<sub>outer</sub> = 8 iterations at a BER of  $10^{-3}$  is shown in Fig. 9. The effective throughput in Bits Per Channel Use (bpcu) for each code rate is also shown. As expected, the Eb/NO gain reduces as the coding

rate increases, since fewer errors can be corrected at higher coding rates. The Eb/NO gain is largest for the configurations with the worst uncoded BER performance, as the coding allows the OTFS and OFDM configurations to overcome the higher diversity gain of AFDM.

11.4

N/A

#### VI. CONCLUSION

10

N/A

10

Iterative soft-MMSE equalisation in conjunction with both RSC and RSC-URC coding has been conceived for AFDM, and both the BER and EXIT chart performance have been compared to that of OFDM and different OTFS configurations. The results recorded for  $R_c = 0.9$  and different variable Sets are summarised in Table 5. The AFDM configurations are shown to exhibit a lower BER at high Eb/NO than their equivalent OTFS counterparts, at lower matrix dimension, at high coding rates, and at low iteration number. This is because AFDM possesses higher degrees of freedom than OTFS, since AFDM is a one-dimensional waveform, whereas OTFS is two-dimensional. When the number of iterations is increased, the BER performance of the AFDM configurations and their equivalent OTFS configurations are shown to be similar. At the communication receiver velocity considered (150 m/s), both AFDM and OTFS tend to outperform OFDM, for both coded and uncoded transmission. Given that the RSC BER performance fails to improve beyond two iterations, this solution is recommended for low-complexity transceivers. By contrast, if the extra complexity of the RSC-URC aided transceiver is affordable, an extra Eb/NO gain of 1.8 dB may be attained at a BER of  $10^{-5}$  and a code rate of 0.5.

Future work will investigate the relative performance of AFDM and OTFS for other coding methods, as well as for ISAC [25], [26], [27], [28], [29], [30], [31], [32], [33]. Other research areas of interest for coded AFDM are satellite communication [8], [43], [44], reconfigurable intelligent surfaces [38], [45], [46], and reconfigurable holographic surfaces [47].

# **REFERENCES**

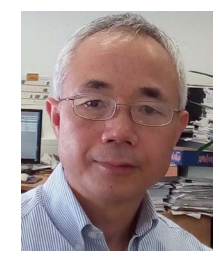
- A. Bemani, N. Ksairi, and M. Kountouris, "AFDM: A full diversity next generation waveform for high mobility communications," in *Proc.* 2021 IEEE Int. Conf. Commun. Workshops, 2021, pp. 1–6.
- [2] T. Erseghe, N. Laurenti, and V. Cellini, "A multicarrier architecture based upon the affine fourier transform," *IEEE Trans. Commun.*, vol. 53, no. 5, pp. 853–862, May 2005.
- [3] X. Ouyang and J. Zhao, "Orthogonal chirp division multiplexing," *IEEE Trans. Commun.*, vol. 64, no. 9, pp. 3946–3957, Sep. 2016.
- [4] M. S. Omar and X. Ma, "Performance analysis of OCDM for wireless communications," *IEEE Trans. Wireless Commun.*, vol. 20, no. 7, pp. 4032–4043, Jul. 2021.

- [5] R. Hadani et al., "Orthogonal time frequency space modulation," in Proc. 2017 IEEE Wireless Commun. Netw. Conf., 2017, pp. 1–6.
- [6] R. Hadani and A. Monk, "OTFS: A new generation of modulation addressing the challenges of 5G," 2018, arXiv:1802.02623.
- [7] Q. Li, J. Li, M. Wen, X. Dang, H. Arslan, and N. Al-Dhahir, "Affine frequency division multiplexing for 6 G networks: Fundamentals, opportunities, and challenges," *IEEE Netw.*, early access, May 13, 2025, doi: 10.1109/MNET.2025.3569668.
- [8] Y. Wang, Y. He, L. Zhao, and Y. Jiang, "AFDM-based preamble sequence transmission for 6G mobile satellite communication systems," *IEEE Trans. Wireless Commun.*, vol. 24, no. 10, pp. 8445-8460, Oct. 2025.
- [9] H. S. Rou and G. T. F. de Abreu, "Chirp-permuted AFDM for quantum-resilient physical-layer secure communications," *IEEE Wireless Commun. Lett.*, vol. 14, no. 8, pp. 2376–2380, Aug. 2025.
- [10] Y. I. Tek and E. Basar, "A novel and secure AFDM system for high mobility environments," *IEEE Trans. Veh. Technol.*, early access, Jul. 7, 2025, doi: 10.1109/TVT.2025.3586731.
- [11] V. Savaux, "Special cases of DFT-based modulation and demodulation for affine frequency division multiplexing," *IEEE Trans. Commun.*, vol. 72, no. 12, pp. 7627–7638, Dec. 2024.
- [12] A. Bemani, G. Cuozzo, N. Ksairi, and M. Kountouris, "Affine frequency division multiplexing for next-generation wireless networks," in *Proc.* 17th Int. Symp. Wireless Commun. Syst., 2021, pp. 1–6.
- [13] A. Bemani, N. Ksairi, and M. Kountouris, "Affine frequency division multiplexing for next generation wireless communications," *IEEE Trans. Wireless Commun.*, vol. 22, no. 11, pp. 8214–8229, Nov. 2023.
- [14] H. Yin, X. Wei, Y. Tang, and K. Yang, "Diagonally reconstructed channel estimation for MIMO-AFDM with inter-doppler interference in doubly selective channels," *IEEE Trans. Wireless Commun.*, vol. 23, no. 10, pp. 14066–14079, Oct. 2024.
- [15] K. Zheng, M. Wen, T. Mao, L. Xiao, and Z. Wang, "Channel estimation for AFDM with superimposed pilots," *IEEE Trans. Veh. Technol.*, vol. 74, no. 2, pp. 3389–3394, Feb. 2025.
- [16] H. Xia, A. Zhang, D. Guo, D. Tian, and S. Wang, "A single-pilot-aided channel estimation scheme based on interference position indices for AFDM in delay-doppler channels," *IEEE Wireless Commun. Lett.*, vol. 14, no. 8, pp. 2466–2470, Aug. 2025.
- [17] H. Yuan et al., "PAPR reduction with pre-chirp selection for affine frequency division multiplexing," *IEEE Wireless Commun. Lett.*, vol. 14, no. 3, pp. 736–740, Mar. 2025.
- [18] V. M. Reddy and H. Bitra, "PAPR in AFDM: Upper bound and reduction with normalized  $\mu$ -law companding," *IEEE Access*, vol. 13, pp. 86553–86561, 2025.
- [19] J. Zhu, Q. Luo, G. Chen, P. Xiao, and L. Xiao, "Design and performance analysis of index modulation empowered AFDM system," *IEEE Wireless Commun. Lett.*, vol. 13, no. 3, pp. 686–690, Mar. 2024.
- [20] Y. Tao, M. Wen, Y. Ge, J. Li, E. Basar, and N. Al-Dhahir, "Affine frequency division multiplexing with index modulation: Full diversity condition, performance analysis, and low-complexity detection," *IEEE J. Sel. Areas Commun.*, vol. 43, no. 4, pp. 1041–1055, Apr. 2025.
- [21] G. Liu et al., "Pre-chirp-domain index modulation for full-diversity affine frequency division multiplexing towards 6 G," *IEEE Trans. Wire-less Commun.*, vol. 27, no. 9, pp. 7331–7345, Sep. 2025.
- [22] M. Qian, F. Ji, Y. Ge, M. Wen, and Y. L. Guan, "Index modulated affine frequency division multiplexing with spread spectrum," *IEEE Trans. Wireless Commun. Letters*, vol. 14, no. 10, pp. 3229–3233, 2025.
- [23] X. Wang, L. Xiao, Q. Luo, J. Zhou, M. Wen, and T. Jiang, "Low-complexity vector-by-vector detector for AFDM-IM systems by reconstructing sparse channel matrix," *IEEE Commun. Lett.*, vol. 28, no. 8, pp. 1839–1843, Aug. 2025.
- [24] Q. Luo et al., "AFDM-SCMA: A promising waveform for massive connectivity over high mobility channels," *IEEE Trans. Wireless Commun.*, vol. 23, no. 10, pp. 14421–14436, Oct. 2024.
- [25] H. S. Rou et al., "From orthogonal time-frequency space to affine frequency-division multiplexing: A comparative study of nextgeneration waveforms for integrated sensing and communications in doubly dispersive channels," *IEEE Signal Process. Mag.*, vol. 41, no. 5, pp. 71–86, Sep. 2024.
- [26] Y. Ni, Z. Wang, P. Yuan, and Q. Huang, "An AFDM-based integrated sensing and communications," in *Proc.* 2022 Int. Symp. Wireless Commun. Syst., 2022, pp. 1–6.
- [27] A. Bemani, N. Ksairi, and M. Kountouris, "Integrated sensing and communications with affine frequency division multiplexing," *IEEE Wireless Commun. Lett.*, vol. 13, no. 5, pp. 1255–1259, May 2024.

- [28] Y. Ni, P. Yuan, Q. Huang, F. Liu, and Z. Wang, "An integrated sensing and communications system based on affine frequency division multiplexing," *IEEE Trans. Wireless Commun.*, vol. 24, no. 5, pp. 3763–3779, May 2025.
- [29] K. R. R. Ranasinghe, H. S. Rou, G. T. Freitas de Abreu, T. Takahashi, and K. Ito, "Joint channel, data, and radar parameter estimation for AFDM systems in doubly-dispersive channels," *IEEE Trans. Wireless Commun.*, vol. 24, no. 2, pp. 1602–1619, Feb. 2025.
- [30] F. Xiao, Z. Li, and D. Slock, "Multipath component power delay profile based joint range and doppler estimation for AFDM-ISAC systems," 2025, arXiv:2503.10833.
- [31] F. Zhang et al., "AFDM-Enabled integrated sensing and communication: Theoretical framework and pilot design," *IEEE J. Sel. Areas Commun.*, pp. 1–1, 2025.
- [32] J. Zhu, Y. Tang, F. Liu, X. Zhang, H. Yin, and Y. Zhou, "AFDM-Based bistatic integrated sensing and communication in static scatterer environments," *IEEE Wireless Commun. Lett.*, vol. 13, no. 8, pp. 2245–2249, Aug. 2024.
- [33] Y. Luo, Y. L. Guan, Y. Ge, D. González G., and C. Yuen, "A novel angle-delay-doppler estimation scheme for AFDM-ISAC system in mixed near-field and far-field scenarios," *IEEE Internet Things J.*, vol. 12, no. 13, pp. 22669–22682, Jul. 2025.
- [34] C. Sturm and W. Wiesbeck, "Waveform design and signal processing aspects for fusion of wireless communications and radar sensing," *Proc. IEEE*, vol. 99, no. 7, pp. 1236–1259, Jul. 2011.
- [35] Z. Li, C. Zhang, G. Song, X. Fang, X. Sha, and D. T. M. Slock, "Chirp parameter selection for affine frequency division multiplexing with MMSE equalization," *IEEE Trans. Commun.*, vol. 73, no. 7, pp. 5079–5093, Jul. 2025.
- [36] X. Li et al., "Affine frequency division multiplexing over wideband doubly-dispersive channels with time-scaling effects," *IEEE Trans. Wireless Commun.*, early access, Jul. 10, 2025, doi: 10.1109/TWC.2025.3584752.
- [37] J. Xu, Z. Liang, and K. Niu, "Multi-block UAMP detection for AFDM under fractional delay-doppler channel," in *Proc. 2025 IEEE Wireless Commun. Netw. Conf.*, 2025, pp. 1–6.
- [38] C. Xu et al., "OTFS-Aided RIS-Assisted SAGIN systems outperform their OFDM counterparts in doubly selective high-doppler scenarios," *IEEE Internet Things J.*, vol. 10, no. 1, pp. 682–703, Jan. 2023.
- [39] C. Xu, S. Sugiura, S. X. Ng, P. Zhang, L. Wang, and L. Hanzo, "Two decades of MIMO design tradeoffs and reduced-complexity MIMO detection in near-capacity systems," *IEEE Access*, vol. 5, pp. 18564–18632, 2017.
- [40] C. Xu, D. Liang, S. Sugiura, S. X. Ng, and L. Hanzo, "Reduced-complexity Approx-Log-Map and Max-Log-MAP soft PSK/QAM detection algorithms," *IEEE Trans. Commun.*, vol. 61, no. 4, pp. 1415–1425, Apr. 2013.
- [41] P. Robertson, E. Villebrun, and P. Hoeher, "A comparison of optimal and sub-optimal MAP decoding algorithms operating in the log domain," in *Proc. IEEE Int. Conf. Commun.*, 1995, vol. 2, pp. 1009–1013.
- [42] L. Hanzo, T. H. Liew, B. L. Yeap, R. Y. S. Tee, and S. X. Ng, "Turbo equalisation for partial-response systems," John Wiley & Sons, Ltd, 2011, pp. 289–323, ch. 10. [Online]. Available: https://onlinelibrary.wiley.com/doi/abs/10.1002/9780470978481.ch10
- [43] X. Qiang, L. You, C. G. Tsinos, W. Wang, X. Gao, and B. Ottersten, "Joint communications and sensing for hybrid massive MIMO LEO satellite systems with beam squint," in *Proc. 2022 IEEE Int. Conf. Commun. Workshops*, 2022, pp. 963–968.
- [44] S. Aliaga, A. J. Alqaraghuli, and J. M. Jornet, "Joint terahertz communication and atmospheric sensing in low earth orbit satellite networks: Physical layer design," in *Proc. IEEE 23rd Int. Symp. World Wireless, Mobile Multimedia Networks*, 2022, pp. 457–463.
- [45] C. Xu et al., "Reconfigurable intelligent surface assisted multi-carrier wireless systems for doubly selective high-mobility Ricean channels," *IEEE Trans. Veh. Technol.*, vol. 71, no. 4, pp. 4023–4041, Apr. 2022.
- [46] C. Pan et al., "Reconfigurable intelligent surfaces for 6 G systems: Principles, applications, and research directions," *IEEE Commun. Mag.*, vol. 59, no. 6, pp. 14–20, Jun. 2021.
- [47] R. Deng, Y. Zhang, H. Zhang, B. Di, H. Zhang, and L. Song, "Reconfigurable holographic surface: A new paradigm to implement holographic radio," *IEEE Veh. Technol. Mag.*, vol. 18, no. 1, pp. 20–28, Mar. 2023.



**HUGO HAWKINS** (Graduate Student Member, IEEE) received the B.Eng. (with First Class Hons.) degree in electrical and electronic engineering in 2021 from the University of Southampton, Southampton, U.K., where he is currently working toward the Ph.D. degree with Next Generation Wireless Research Group. His research interests include integrated sensing and communication.



**LIE-LIANG YANG** (Fellow, IEEE) is currently a Professor of wireless communications with the University of Southampton, Southampton, U.K. He has authored or coauthored more than 400 research papers and four books. His research interests include wireless communications, wireless networks, signal processing for wireless communications, molecular communications and nano-networks. He is a Fellow of IET, AAIA, and AIIA.



**CHAO XU** (Senior Member, IEEE) is currently a Senior Lecturer with Next Generation Wireless Research Group, University of Southampton, Southampton, U.K. His research interests include integrated sensing and communication, optical wireless, and quantum key distribution. He was the recipient of the 2023 Marie Sklodowska-Curie Actions Global Postdoctoral Fellowships with the highest evaluation score of 100/100.



LAJOS HANZO (Life Fellow, IEEE) received the Honorary Doctorates from the Technical University of Budapest, Budapest, Hungary, in 2009, and Edinburgh University, Edinburgh, U.K., in 2015. He is currently a Foreign Member of the Hungarian Science-Academy, fellow of the Royal Academy of Engineering (FREng), of the IET, of EURASIP. He was the recipient of IEEE Eric Sumner Technical Field Award. For further details please see: http://www-mobile.ecs.soton.ac.uk, https://en.wikipedia.org/wiki/Lajos Hanzo